materials

MDPI

Article

Microwave-Assisted Hydrothermal Synthesis of Zinc-Aluminum Spinel $ZnAl_2O_4$

Tomasz Strachowski [1,*], Ewa Grzanka [2], Jan Mizeracki [2], Adrian Chlanda [1], Magdalena Baran [1], Marcin Małek [3] and Marlena Niedziałek [3]

[1] Research Group of Graphene and Composites, Lukasiewicz Research Network–Institute of Microelectronics and Photonics IMiF, Al. Lotnikow 32/46, 02-668 Warsaw, Poland; adrian.chlanda@imif.lukasiewicz.gov.pl (A.C.); magdalena.baran@imif.lukasiewicz.gov.pl (M.B.)
[2] Institute of High Pressure Physics PAS "Unipress", Sokolowska 29/37, 01-142 Warsaw, Poland; elesk@unipress.waw.pl (E.G.); janekm@unipress.waw.pl (J.M.)
[3] Faculty of Civil Engineering and Geology, Military University of Technology, ul. Gen. Sylwestra Kaliskiego 2, 00-908 Warsaw, Poland; marcin.malek@wat.edu.pl (M.M.); marlena.niedzialek@wat.edu.pl (M.N.)
* Correspondence: tomasz.strachowski@imif.lukasiewicz.gov.pl

Abstract: The drawback of the hydrothermal technique is driven by the fact that it is a time-consuming operation, which greatly impedes its commercial application. To overcome this issue, conventional hydrothermal synthesis can be improved by the implementation of microwaves, which should result in enhanced process kinetics and, at the same time, pure-phase and homogeneous products. In this study, nanometric zinc aluminate ($ZnAl_2O_4$) with a spinel structure was obtained by a hydrothermal method using microwave reactor. The average $ZnAl_2O_4$ crystallite grain size was calculated from the broadening of XRD lines. In addition, BET analysis was performed to further characterize the as-synthesized particles. The synthesized materials were also subjected to microscopic SEM and TEM observations. Based on the obtained results, we concluded that the grain sizes were in the range of 6–8 nm. The surface areas measured for the samples from the microwave reactor were 215 and 278 $m^2\ g^{-1}$.

Keywords: zinc-aluminum spinel $ZnAl_2O_4$; hydrothermal synthesis; microwave reactor

Citation: Strachowski, T.; Grzanka, E.; Mizeracki, J.; Chlanda, A.; Baran, M.; Małek, M.; Niedziałek, M. Microwave-Assisted Hydrothermal Synthesis of Zinc-Aluminum Spinel $ZnAl_2O_4$. *Materials* **2022**, *15*, 245. https://doi.org/10.3390/ma15010245

Academic Editor: Aivaras Kareiva

Received: 3 December 2021
Accepted: 28 December 2021
Published: 29 December 2021

1. Introduction

Spinels are a group of compounds with the general formula AB_2O_4, where A is a divalent metal (Zn, Mg, Fe or Mn) and B is a trivalent metal (Al, Fe, Cr or Mn). The spinel network cell is regular. It can be described as consisting of a series of F-type networks (embedded corners and wall centers). A regular elementary cell contains 32 oxygen anions and 24 cations: 8 (A)-type cations occupy tetrahedral gaps, and 16 (B)-type cations are in octahedral gaps. In regular spinels (which include $ZnAl_2O_4$), the tetrahedral positions are occupied by 8 A(+III) ions, and the octahedral positions are occupied by 16 B(+III) ions [1–5].

Zinc-aluminum spinel can be obtained by various methods, such as sol–gel [6–12], hydrothermal methods [13–20], co-precipitation [21–26], combustion methods [27–30] and solvothermal synthesis [31–33]. Implementation of these methods resulted in splines with a size distribution ranging from 15 to 100 nm. It is worth noting that hydrothermal synthesis is the simplest method to obtain spinels with nanometric grain size. However, this method usually needs a long process time and low temperature. Conventional hydrothermal synthesis can be improved by the implementation of microwaves, which results in a faster increase in temperature and process kinetics and the generation of pure-phase and homogeneous products.

Oxide spinels comprise a broad group of compounds with complex structures that are of great technological importance. This group includes zinc-aluminum spinel, which is

characterized by many desirable properties, including: high mechanical resistivity, high thermal stability and low sintering temperature. Zinc-aluminum spinel is widely used in chemical and electronics industries and in catalytic reactions such as cracking, dehydration, hydrogenation and dehydrogenation. This applies mainly to spinel doped with Fe(+III) ions [34–40]. The zinc-aluminum spinel is transparent to light at wavelengths above 320 nm and has therefore found application in optoelectronics (energy gap 3.8 eV) [41–50]. In addition, transparent spinels without defects are used in precision mechanics (e.g., for bearing production) and as gemstones [51–55]. This spinel has also found applications in the manufacture of nanotubes, nanowires and thin films. Zinc-aluminum spinel doped with ions of various chemical elements, such as Co^{3+}, Er^{3+}, Eu^{3+}, Yb^{3+}, Tb^{3+} and Mn^{3+}, also has interesting properties. Spinel doped with these elements exhibits excellent luminescent properties [56–65].

This manuscript contains a detailed description of the synthesis and characterization of selected vital properties of as-obtained materials. Although one can find literature reports describing scientific efforts aimed at fabricating similar materials, it is worth underlining that it is hard to obtain zinc-aluminum spinel grains characterized by small sizes (in a range of single nanometers). There are several literature reports of obtaining zinc-aluminum spinel with sizes measured in single nanometers [7,19].

In addition to zinc-aluminum spinel, other compounds in the spinel group, such as $ZnGa_2O_4$ [66], $MgCr_2O_4$ [67] and $SrAl_2O_4$ [68], are of great interest.

The authors consider the most interesting achievement of this research to be the preparation of zinc-aluminum spinel with a small grain size and large specific surface area. In the literature, one can find zinc-aluminum spinels with much larger grains [6,11–13,18].

2. Materials and Methods

2.1. Materials

$Zn(NO_3)_2$*$6H_2O$ and $Al(NO_3)_3$*$9H_2O$ were used for the hydrothermal synthesis of zinc-aluminum spinel. A 2 M aqueous solution of KOH was used as the substance for the precipitation of zinc and aluminum hydroxides. When preparing the solution of the respective salts, the proportion was maintained so that the molar ratio of Al:Zn was 2:1.

Appropriate amounts of zinc and aluminum salts were weighed in a 500 mL beaker, and then 150 mL of distilled water was added. Mixing was carried out with a magnetic stirrer at room temperature for 1 h. A 2 M KOH aqueous solution was gradually poured into the mixed solution until pH = 12 was reached. Figure 1 shows a schematic step-by-step description of the production of zinc-aluminum spinel.

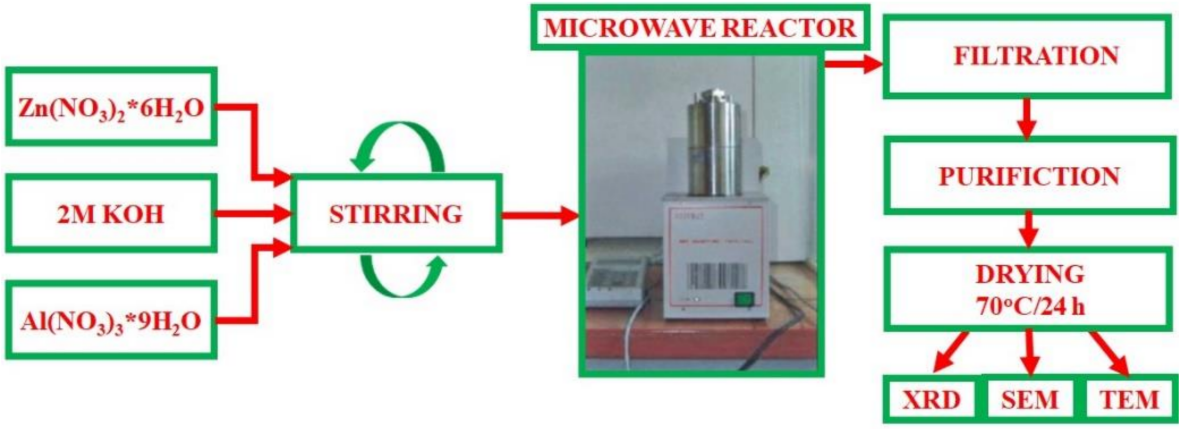

Figure 1. Scheme of the production of zinc-aluminum spinel.

The obtained zinc-aluminum hydroxide suspension was poured into reaction vessels and placed in a microwave reactor. The microwave reactor is a laboratory instrument designed for hydrothermal syntheses in a microwave field. Microwave energy is drawn

into the head from the magnetron through a waveguide in which a short antenna is immersed. The whole system is controlled by means of a central processing unit (CPU) controller communicating with a personal computer (PC). The computer program allows adjusting power thresholds and pressure limits, along with temperature and pressure registration during the process [69].

The experiment in the microwave reactor was as follows. The prepared solution was poured into a Teflon reaction vessel with a capacity of 110 mL. The vessel was then closed with a Teflon lid and placed inside the stainless-steel head. The final step was to close the head and start the process.

The appropriate process parameters must be set in order to obtain good-quality resulting material. In the case of the presented study, the process was conducted for 15, 30 or 60 min. After completion of the processes, the product was filtered under pressure through filters and washed repeatedly with distilled water. The purified material was then placed in a vacuum dryer (70 °C/24 h).

2.2. Methods

A Siemens D-5000 X-ray diffractometer (Siemens-Bruker Corporation, Germany) was used to analyze the obtained synthesis products. It enables the determination of the phase composition, recognition of crystallographic lattice and identification of the coordinates of atoms in the elementary cell (by the Rietveld method).

Density was determined by a gas pycnometer (AccuPyc 1330 helium pycnometer, Micromeritics, Norcross, GA, USA). The specific surface area was measured using the BET adsorption method with a Micromeritics device. Microstructure studies of nanopowders were performed using scanning microscopy with a Zeiss LEO1530 (Carl Zeiss, Germany) equipped with a Zeiss Gemini column.

3. Results and Discussion

X-ray Tomography of Ceramic Preforms

Table 1 presents the results of tests on zinc-aluminum spinel obtained in the microwave reactor. The overriding conclusion from these results is that the grain size was in the same range (6–7 nm), and it was independent of the synthesis time. The process temperature was approximately 200 °C. The density and specific surface areas were maintained at similar levels.

Table 1. Results of zinc-aluminum spinel analysis.

Time (min)	15	30	60
Pressure (atm)	39	39	39
Density (g/cm^3)	3.72	3.53	3.68
BET (m^2/g)	260	266	262
Grain size (nm)	6–7	6–7	6–7
Phases	$ZnAl_2O_4$ + ZnO	$ZnAl_2O_4$ + ZnO	$ZnAl_2O_4$ + ZnO

XRD analysis revealed that the microwave reactor yielded a product that contained a ZnO phase in addition to the $ZnAl_2O_4$ spinel phase. In order to obtain a pure spinel phase, we decided to perform an experiment using the same process time while increasing the process pressure (50, 60 and 70 atm). Figure 2 shows the results of XRD analysis for samples obtained at different pressures for 30 min. It can be observed that as the pressure increased, the ZnO phase disappeared, and the pure $ZnAl_2O_4$ phase remained.

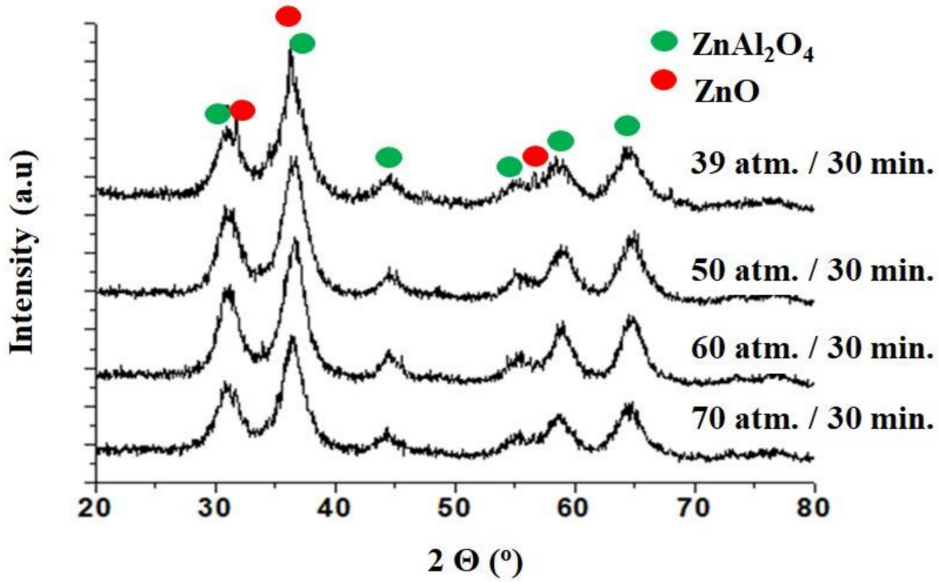

Figure 2. XRD analysis of zinc-aluminum spinel under different pressures.

Table 2 shows the results of the analysis of zinc-aluminum spinel samples that were synthesized at elevated pressure. It was observed that as the pressure and time process increased, the ZnO phase disappeared, and the pure $ZnAl_2O_4$ phase remained.

Table 2. Results of the analysis of zinc-aluminum spinel samples after synthesis.

Sample	Density (g/cm^3)	BET (m^2/g)	Grain Size (nm)	Phases
15 min/50 atm	3.41	271	7	$ZnAl_2O_4$
15 min/60 atm	3.41	254	7	$ZnAl_2O_4$
15 min/70 atm	3.42	242	7	$ZnAl_2O_4$
30 min/50 atm	3.53	278	6	$ZnAl_2O_4$
30 min/60 atm	3.53	255	8	$ZnAl_2O_4$
30 min/70 atm	3.51	260	6	$ZnAl_2O_4$
60 min/50 atm	3.48	266	6	$ZnAl_2O_4$
60 min/60 atm	3.51	260	6	$ZnAl_2O_4$
60 min/70 atm	3.48	223	7	$ZnAl_2O_4$

Figure 3 shows the dependence of the specific surface area (BET) as a function of process time and pressure. It can be observed that the highest value was achieved for the sample obtained in the 30 min process at a pressure of 50 atm. As the pressure and process time increased, the value of the specific surface area decreased. This is particularly evident for samples obtained at 60 min of process time. This was significantly influenced by lowering the process temperature, increasing the pressure and using microwaves, which also shortened the process time. Based on the literature review [6–8,12–15,20,21], it can be noted that previous studies carried out the synthesis of $ZnAl_2O_4$ in the temperature range from 600 to 900 °C. At those temperatures, a product with a small specific surface area and, consequently, a large grain size was obtained.

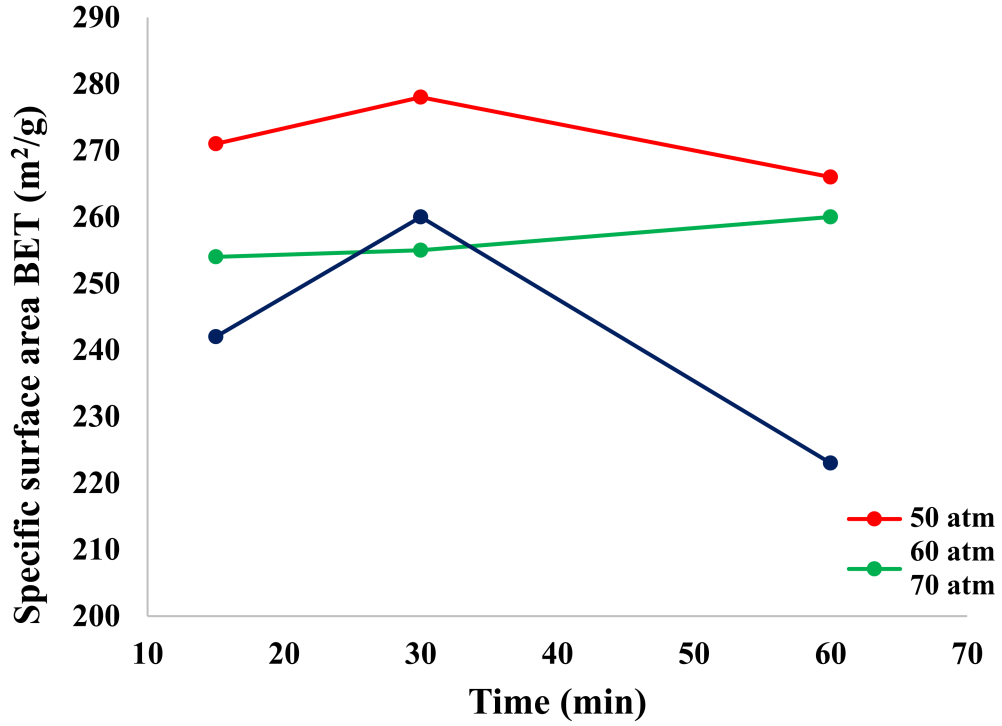

Figure 3. Dependence of the specific surface area as a function of process time and pressure.

Figure 4 shows the dependence of density on pressure and process time. It can be observed that with an increase in these parameters (up to 30 min), the density increased, while after this time, it decreased.

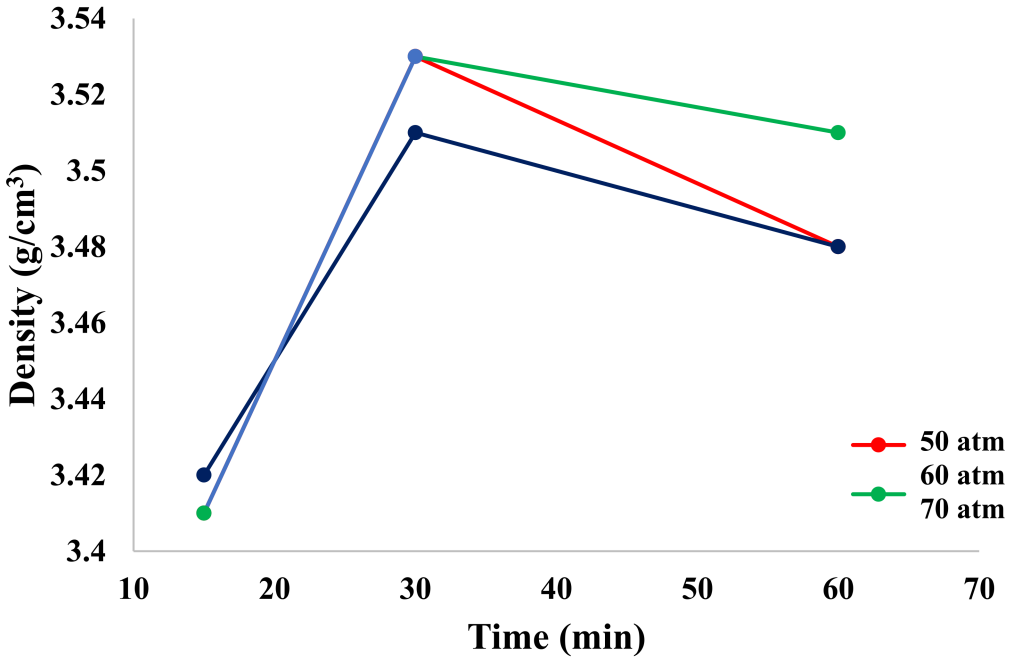

Figure 4. Dependence of density on pressure and process time.

After measuring the density and specific surface area with the BET method, it was found that 30 min was the optimal process time, as both parameters (density and specific surface area) were characterized by the highest values.

Figure 5 shows scanning microscope (SEM) and transmission microscope photographs (Figure 6) for samples obtained at the optimum process time of 30 min. One can notice the powder crystallites in the form of spherical grains. Observation by transmission microscopy confirmed the actual nanometric grain size obtained in this study.

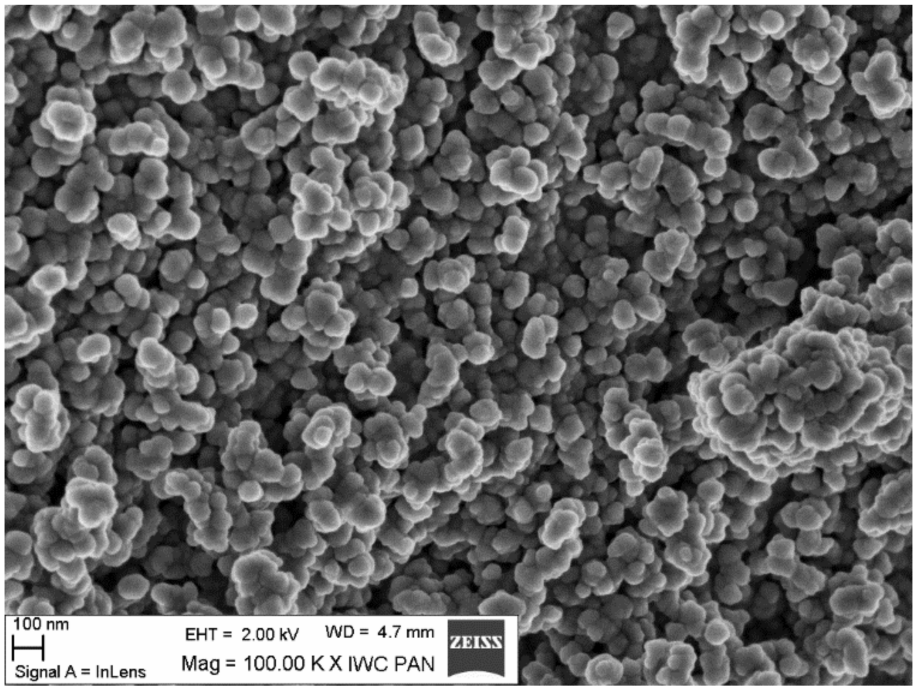

(**a**) 30 min/39 atm

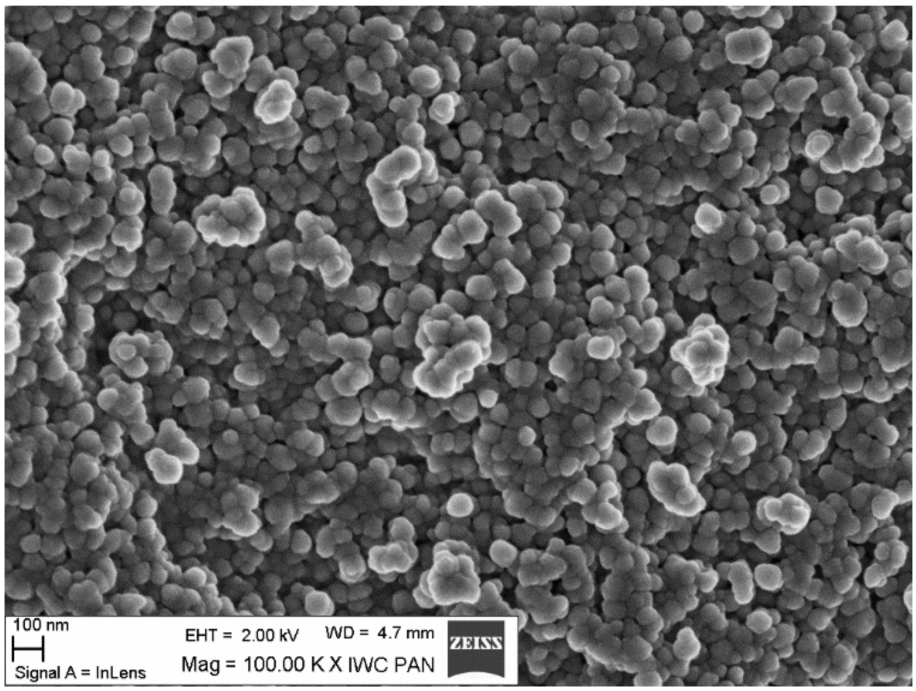

(**b**) 30 min/50 atm

Figure 5. *Cont.*

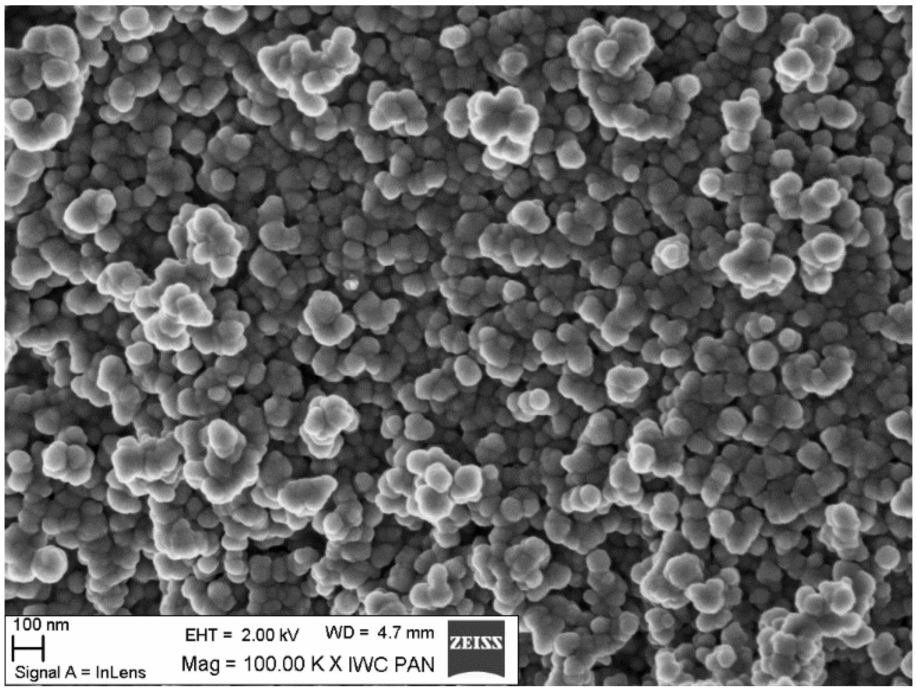

(**c**) 30 min/60 atm

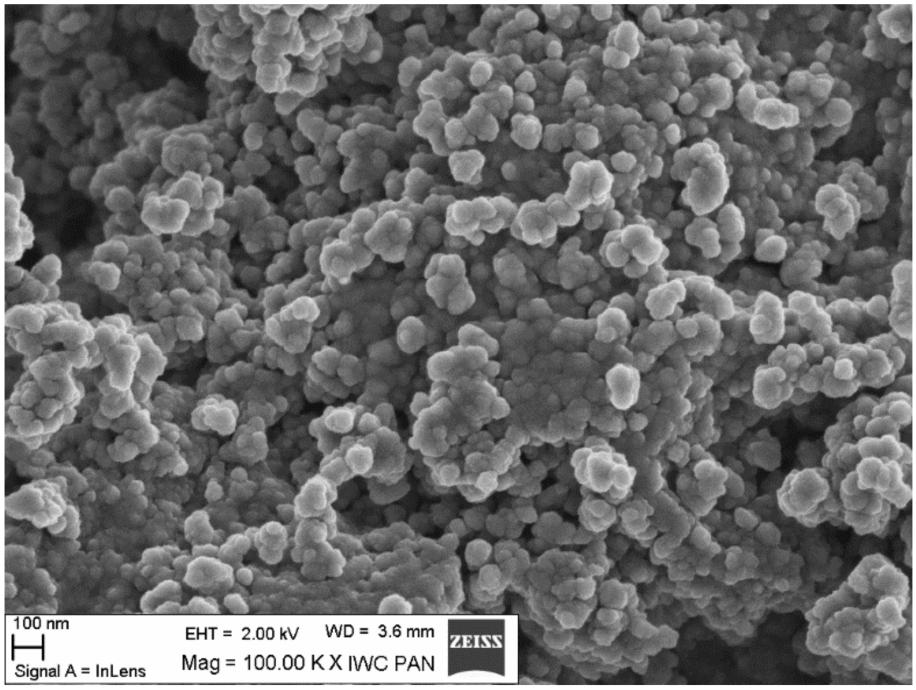

(**d**) 30 min/70 atm

Figure 5. SEM pictures of samples obtained at the optimum process time of 30 min.

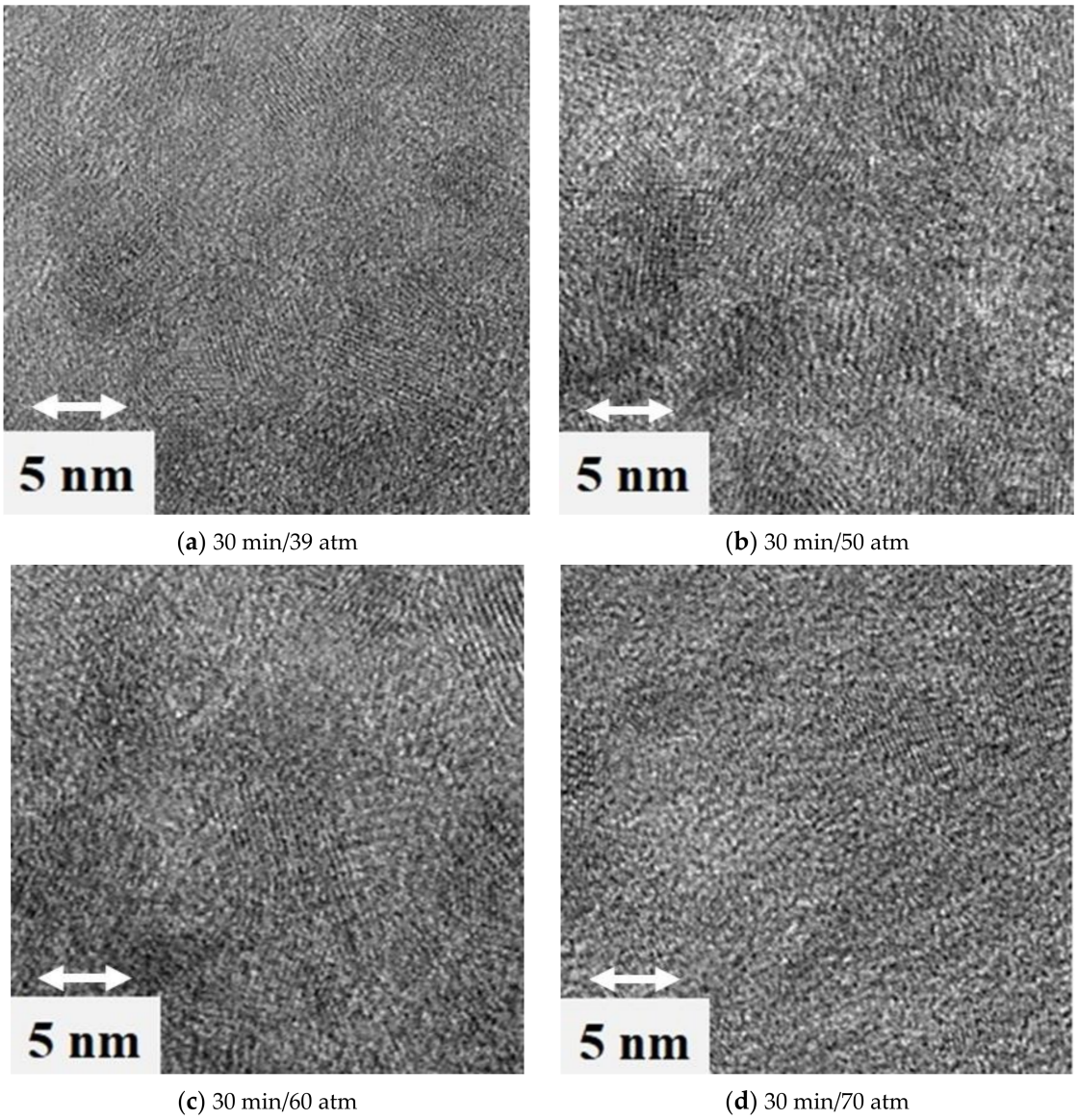

(**a**) 30 min/39 atm (**b**) 30 min/50 atm

(**c**) 30 min/60 atm (**d**) 30 min/70 atm

Figure 6. TEM pictures of samples obtained at the optimum process time of 30 min.

Based on the obtained results, it can be concluded that in a single synthesis, zinc-aluminum spinel was obtained with a grain size in the range of 6–8 nm and a density in the range of 3.41–3.51 g/cm^3.

4. Conclusions

Hydrothermal synthesis of zinc-aluminum spinel using a microwave reactor was carried out.

We concluded that the syntheses performedin the microwave reactor resulted in zinc-aluminum spinel with an average grain size in the range of 6–7 nm. At a lower pressure (39 atm), a ZnO phase appeared in addition to the spinel phase, which in this case, was unwanted. In order to obtain a pure spinel phase (without ZnO doping), the process pressure was increased (50, 60 and 70 atm).

The obtained products were characterized by a high specific surface area in the range of 220–280 m^2/g. The density measured on a helium pycnometer was in the range of 3.4–3.7 g/cm^3. The aforementioned material properties were plotted against time, which enabled the designation of the optimum process time: 30 min.

Analysis of the morphology using a scanning microscope showed that the reaction product agglomerated as beads (Figure 5). These structures were composed of fine crystallites that were attracted to each other in the reaction slurry or during post-synthesis washing. The morphology of the powders observed with a transmission microscope (TEM) enclosed fine grains (below 10 nm). We concluded that the higher the process pressure, the smaller the grains. The finest grains were observed for powder obtained at a pressure of 70 atm and a time of 30 min.

Having all of this in mind, we want to underline that the synthesis of zinc-aluminum spinel using a hydrothermal method using a microwave reactor is advantageous because it results in a final product with:

- High density;
- Phase homogeneity;
- Nanometric grain size.

Author Contributions: Conceptualization, T.S.; methodology, T.S., M.B., E.G., J.M. and M.N.; validation, A.C. and M.M.; investigation, E.G., J.M., M.N. and M.B.; resources, writing—original draft preparation, T.S.; writing—review and editing, A.C. and M.M. All authors have read and agreed to the published version of the manuscript.

Funding: Institute of High Pressure Physics of the Polish Academy of Sciences (statutory project). Faculty of Civil Engineering and Geodesy of the Military University of Technology as part of project UGB No. 22-870.

Institutional Review Board Statement: Not applicable.

Informed Consent Statement: Not applicable.

Data Availability Statement: All individuals included in this section have agreed to be confirmed.

Acknowledgments: The research was financed by the own funds of the Institute of High Pressure Physics of the Polish Academy of Sciences. This work was financially supported by the Faculty of Civil Engineering and Geodesy of the Military University of Technology as part of project UGB No. 22-870.

Conflicts of Interest: The authors declare no conflict of interest.

References

1. Bosi, F.; Biagioni, C.; Pasero, M. Nomenclature and classification of the spinel supergroup. *Eur. J. Mineral.* **2019**, *31*, 183–192. [CrossRef]
2. O'Neill, H.S.C.; Navrotsky, A. Simple spinels: Crystallographic parameters, cation radii, lattice energies, and cation distribution. *Am. Mineral.* **1983**, *68*, 181–194.
3. Hill, R.J.; Craig, J.R.; Gibbs, G.V. Systematics of the Spinel Structure Type. *Phys. Chem. Miner.* **1979**, *4*, 317. [CrossRef]
4. Sommer, S.; Drath Bøjesen, E.; Lock, N.; Kasai, H.; Skibsted, J.; Nishibori, E.; Iversen, B.B. Probing the validity of the spinel inversion model: A combined SPXRD, PDF, EXAFS and NMR study of $ZnAl_2O_4$. *Dalton Trans.* **2020**, *49*, 13449. [CrossRef]
5. Seko, A.; Oba, F.; Tanaka, I. Classification of spinel structures based on first-principles cluster expansion analysis. *Phys. Rev. B* **2010**, *81*, 054114. [CrossRef]
6. Da Silva, A.A.; de Souza Goncalves, A.; Davolos, M.R. Characterization of nanosized $ZnAl_2O_4$ spinel synthesized by the sol–gel method. *J. Sol-Gel Sci. Technol.* **2009**, *49*, 101–105. [CrossRef]
7. Sharma, R.K.; Ghosen, R. Synthesis and characterization of nanocrystalline zinc aluminate spinel powder by sol–gel method. *Ceram. Int.* **2014**, *40*, 3209–3214. [CrossRef]
8. Davar, F.; Salavati-Niasari, M. Synthesis and characterization of spinel-type zinc aluminate nanoparticles by a modified sol–gel method using new precursor. *J. Alloys Compd.* **2011**, *509*, 2487–2492. [CrossRef]
9. Zulfakar, M.S.; Abdullah, H.; Jalal, W.N.W.; Zainuddin, Z.; Shaari, S. Study of Nanocrystalline $ZnAl_2O_4$ and $ZnFe_2O_4$ with SiO_2 on Structural and Optical Properties Synthesized by Sol-Gel Method. *Adv. Mater. Res.* **2015**, *1119*, 96–100. [CrossRef]
10. Valenzuela, M.A.; Bosch, E.; Aguilar-Rios, G.; Montoya, A.; Schifter, I. Comparison Between Sol-Gel, Coprecipitation and Wet Mixing Synthesis of $ZnAl_2O_4$. *J. Sol-Gel Sci. Technol.* **1997**, *8*, 107–110. [CrossRef]
11. Wei, X.; Chen, D. Synthesis and characterization of nanosized zinc aluminate spinel by sol–gel technique. *Mater. Lett.* **2006**, *60*, 823–827. [CrossRef]
12. Belyaev, A.V.; Lelet, M.I.; Kirillova, N.I.; Khamaletdinova, N.M.; Boldin, M.S.; Murashov, A.A.; Balabanov, S.S. Sol-gel synthesis and characterization of $ZnAl_2O_4$ powders for transparent ceramics. *Ceram. Int.* **2019**, *45*, 4835–4839. [CrossRef]

13. Confalonieri, G.; Rotiroti, N.; Bernasconi, A.; Dapiaggi, M. Structural Study of Nano-Sized Gahnite ($ZnAl_2O_4$): From the Average to the Local Scale. *Nanomaterials* **2020**, *10*, 824. [CrossRef]
14. Mathur, S.; Veith, M.; Haas, M.; Shen, H.; Lecerf, N.; Huch, V.; Hufner, S.; Haberkorn, R.; Beck, H.P.; Jilavi, M. Single-Source Sol–Gel Synthesis of Nanocrystalline $ZnAl_2O_4$: Structural and Optical Properties. *J. Am. Ceram. Soc.* **2001**, *84*, 1921–1928. [CrossRef]
15. De Macedo, H.P.; de Araújo Medeiros, R.L.B.; de Medeiros, A.L.; de Oliveira, A.A.S.; de Figueredo, G.P.; de Freitas Melo, M.A.; de Araújo Melo, D.M. Characterization of $ZnAl_2O_4$ Spinel Obtained by Hydrothermal and Microwave Assisted Combustion Method: A Comparative Study. *Mater. Res.* **2017**, *20* (Suppl. S2), 29–33. [CrossRef]
16. Miron, I.; Enache, C.; Vasile, M.; Grozescu, I. Optical properties of $ZnAl_2O_4$ nanomaterials obtained by the hydrothermal method. *Phys. Scr.* **2012**, *T149*, 014064. [CrossRef]
17. Sibera, D.; Strachowski, T.; Lojkowski, W.; Narkiewicz, U.; Chudoba, T.; Jędrzejewski, R.; Majcher, A.; Presz, A. Nano-$ZnAl_2O_4$—Hydrothermal MW Assisted Synthesis In A Stop-Flow Reactor And Characterization. *Maint. Probl.* **2010**, *4*, 91–102.
18. Zawadzki, M. Synthesis of nanosized and microporous zinc aluminate spinel by microwave assisted hydrothermal method (microwave–hydrothermal synthesis of $ZnAl_2O_4$). *Solid State Sci.* **2006**, *8*, 14–18. [CrossRef]
19. Chen, X.Y.; Ma, C.; Zhang, Z.J.; Wang, B.N. Ultrafine gahnite ($ZnAl_2O_4$) nanocrystals: Hydrothermal synthesis and photoluminescent properties. *Mater. Sci. Eng. B* **2008**, *151*, 224–230. [CrossRef]
20. Chen, Z.; Shi, E.; Zheng, Y.; Li, W.; Wu, N.; Zhong, W. Synthesis of mono-dispersed $ZnAl_2O_4$ powders under hydrothermal conditions. *Mater. Lett.* **2002**, *56*, 601–605. [CrossRef]
21. Battistona, S.; Rigoa, C.; da Cruz Severoa, E.; Mazuttia, M.A.; Kuhna, R.C.; Gündelb, A.; Foletto, E.L. Synthesis of Zinc Aluminate ($ZnAl_2O_4$) Spinel and its Application as Photocatalyst. *Mater. Res.* **2014**, *17*, 734–738. [CrossRef]
22. Marconato Stringhini, F.; Foletto, E.L.; Sallet, D.; Assumpção Bertuol, D.; Chiavone-Filho, O.; Oller do Nascimento, C.A. Synthesis of porous zinc aluminate spinel ($ZnAl_2O_4$) by metal-chitosan complexation method. *J. Alloys Compd.* **2014**, *588*, 305–309. [CrossRef]
23. Farhadi, S.; Panahandehjoo, S. Spinel-type zinc aluminate ($ZnAl_2O_4$) nanoparticles prepared by the co-precipitation method: A novel, green and recyclable heterogeneous catalyst for the acetylation of amines, alcohols and phenols under solvent-free conditions. *Appl. Catal. A Gen.* **2010**, *382*, 293–302. [CrossRef]
24. Foletto, E.L.; Battiston, S.; Simoes, J.M.; Moro Bassaco, M.; Severo Fagundes Pereira, L.; Marlon de Moraes Flores, E.; Irineu Muller, E. Synthesis of $ZnAl_2O_4$ nanoparticles by different routes and the effect of its pore size on the photocatalytic process. *Microporous Mesoporous Mater.* **2012**, *163*, 29–33. [CrossRef]
25. Ge, D.-L.; Fan, Y.-J.; Qi, C.-L.; Sun, Z.-X. Facile synthesis of highly thermostable mesoporous $ZnAl_2O_4$ with adjustable pore size. *J. Mater. Chem. A* **2013**, *1*, 1651. [CrossRef]
26. Ananda, G.T.; Kennedya, L.J.; Vijayac, J.J.; Kaviyarasana, K.; Sukumar, M. Structural, optical and magnetic characterization of $Zn_{1-x}Ni_xAl_2O_4$ ($0 \leq x \leq 5$) spinel nanostructures synthesized by microwave combustion technique. *Ceram. Int.* **2015**, *41*, 603–615. [CrossRef]
27. Mirbagheri, S.A.; Masoudpanah, S.M.; Alamolhod, S. Structural and optical properties of $ZnAl_2O_4$ powders synthesized by solution combustion method: Effects of mixture of fuels. *Optik* **2020**, *204*, 164170. [CrossRef]
28. Mohanty, P.; Mohapatro, S.; Mahapatra, R.; Mishra, D.K. Low cost synthesis route of spinel $ZnAl_2O_4$. *Mater. Today Proc.* **2021**, *35*, 130–132. [CrossRef]
29. Ianos, R.; Lazau, R.; Lazau, I.; Pacurariu, C. Chemical oxidation of residual carbon from $ZnAl_2O_4$ powders prepared by combustion synthesis. *J. Eur. Ceram. Soc.* **2012**, *32*, 1605–1611. [CrossRef]
30. Han, M.; Wang, Z.; Xu, Y.; Wu, R.; Jiao, S.; Chen, Y.; Feng, S. Physical properties of $MgAl_2O_4$, $CoAl_2O_4$, $NiAl_2O_4$, $CuAl_2O_4$, and $ZnAl_2O_4$ spinels synthesized by a solution combustion method. *Mater. Chem. Phys.* **2018**, *215*, 251–258. [CrossRef]
31. Sirikajorn, T.; Mekasuwandumrong, O.; Praserthdam, P.; Goodwin, J.G., Jr.; Panpranot, J. Effect of Support Crystallite Size on Catalytic Activity and Deactivation of Nanocrystalline $ZnAl_2O_4$-Supported Pd Catalysts in Liquid-Phase Hydrogenation. *Catal. Lett.* **2008**, *126*, 313–318. [CrossRef]
32. Song, X.; Zheng, S.; Zhang, J.; Li, W.; Chen, Q.; Cao, B. Synthesis of monodispersed $ZnAl_2O_4$ nanoparticles and their tribology properties as lubricant additives. *Mater. Res. Bull.* **2012**, *47*, 4305–4310. [CrossRef]
33. Zawadzki, M. Pd and $ZnAl_2O_4$ nanoparticles prepared by microwave-solvothermal method as catalyst precursors. *J. Alloys Compd.* **2007**, *439*, 312–320. [CrossRef]
34. Ghorbani-Choghamarani, A.; Mohammadi, M.; Shiri, L.; Taherinia, Z. Synthesis and characterization of spinel $FeAl_2O_4$ (hercynite) magnetic nanoparticles and their application in multicomponent reactions. *Res. Chem. Intermed.* **2019**, *45*, 5705–5723. [CrossRef]
35. Enhessari, M. $FeAl_2O_4$ Nanopowders; Structural Analysis and Band Gap Energy. *High Temp. Mater. Proc.* **2017**, *36*, 789–793. [CrossRef]
36. Azam, M.; Nairan, A.; Riaz, S.; Naseem, S. $FeAl_2O_4$ thin films prepared by sol-gel—structural and magnetic properties. *Mater. Today Proc.* **2015**, *2*, 5150–5154. [CrossRef]
37. Jastrzębska, I.; Szczerba, J.; Błachowski, A.; Stoch, P. Structure and microstructure evolution of hercynite spinel ($Fe^{2+}Al_2O_4$) after annealing treatment. *Eur. J. Mineral.* **2017**, *29*, 63–72. [CrossRef]
38. Daghetta, M.A.A.; Dapiaggi, M.; Pellegrino, L.; Pastore, B.; Pagliari, L.; Mazzocchia, C.V. Synthesis of Hercynite at very Mild Condition. *Chem. Eng. Trans.* **2015**, *43*, 1741–1746. [CrossRef]

39. Nestola, F.; Periotto, B.; Anzolini, C.; Andreozzi, G.B.; Woodland, A.B.; Lenaz, D.; Alvaro, M.; Princivalle, F. Equation of state of hercynite, $FeAl_2O_4$, and high-pressure systematics of Mg-Fe-Cr-Al spinels. *Mineral. Mag.* **2015**, *79*, 285–294. [CrossRef]
40. Castillo Rodriguez, G.A.; Garcıa Guillen, G.; Mendivil Palma, M.I.; Das Roy, T.K.; Guzman Hernandez, A.M. Synthesis and Characterization of Hercynite Nanoparticles by Pulsed Laser Ablation in Liquid Technique. *Int. J. Appl. Ceram. Technol.* **2014**, *12*, E34–E43. [CrossRef]
41. Hou, Q.; Meng, F.; Sun, J. Electrical and optical properties of Al-doped ZnO and $ZnAl_2O_4$ films prepared by atomic layer deposition. *Nanoscale Res. Lett.* **2013**, *8*, 144. [CrossRef]
42. Kim, B.-N.; Hiraga, K.; Jeong, A.; Hu, C.; Suzuki, T.S.; Yun, J.-D.; Sakka, Y. Transparent $ZnAl_2O_4$ ceramics fabricated by spark plasma sintering. *J. Ceram. Soc. Jpn.* **2014**, *122*, 784–787. [CrossRef]
43. Guo, Y.; Lu, Y.; Liu, C.; Wang, J.; Han, J.; Ruan, J. Effect of $ZnAl_2O_4$ crystallization on ion-exchange properties in aluminosilicate glass. *J. Alloys Compd.* **2021**, *851*, 156891. [CrossRef]
44. Salih, E.Y.; Mohd Sabri, M.F.; Sulaiman, K.; Hussein, M.Z.; Said, S.M.; Usop, R.; Mohd Salleh, M.F.; Bashir Ali Bashir, M. Thermal, structural, textural and optical properties of $ZnO/ZnAl_2O_4$ mixed metal oxide-based Zn/Al layered double hydroxide. *Mater. Res. Express* **2018**, *5*, 116202. [CrossRef]
45. Iaiche, S.; Djelloul, A. $ZnO/ZnAl_2O_4$ Nanocomposite Films Studied by X-ray Diffraction, FTIR, and X-ray Photoelectron Spectroscopy. *J. Spectrosc.* **2015**, *2015*, 836859. [CrossRef]
46. Salih, E.Y.; Mohd Sabri, M.F.; Hussein, M.Z.; Sulaiman, K.; Mohd Said, S.; Saifullah, B.; Bashir Ali Bashir, M. Structural, optical and electrical properties of $ZnO/ZnAl_2O_4$ nanocomposites prepared via thermal reduction approach. *J. Mater. Sci.* **2018**, *53*, 581–590. [CrossRef]
47. Chandramohan, R.; Dhanasekaran, V.; Arumugam, R.; Sundaram, K.; Thirumalai, J.; Mahalingam, T. Physical Properties Evaluation Of Annealed $ZnAl_2O_4$ Alloy Thin Films. *Dig. J. Nanomater. Biostructures* **2012**, *7*, 1315–1325.
48. Kumar, K.; Ramamoorthy, K.; Koinkar, P.M.; Chandramohan, R.; Sankaranarayan, K. A novel in situ synthesis and growth of $ZnAl_2O_4$ thin films. *J. Cryst. Growth* **2006**, *289*, 405–407. [CrossRef]
49. Somraksa, W.; Suwanboon, S.; Amornpitoksuk, P.; Randorn, C. Physical and Photocatalytic Properties of $CeO_2/ZnO/ZnAl_2O_4$ Ternary Nanocomposite Prepared by Co-precipitation Method. *Mater. Res.* **2020**, *23*, e20190627. [CrossRef]
50. Iaiche, S.; Boukaous, C.; Alamarguy, D.; Djelloul, A.; Hamana, D. Effect of Solution Concentration on $ZnO/ZnAl_2O_4$ Nanocomposite Thin Films Formation Deposited by Ultrasonic Spray Pyrolysis on Glass and Si(111) Substrates. *J. Nano Res.* **2020**, *63*, 10–30. [CrossRef]
51. Gorghinian, A.; Mottana, A.; Rossi, A.; Oltean, F.M.; Esposito, A.; Marcelli, A. Investigating the colour of spinel: 1. Red gem-quality spinels ("balas") from Ratnapura (Sri Lanka). *Rend. Lincei* **2013**, *24*, 127–140. [CrossRef]
52. Phyo, M.M.; Bieler, E.; Franz, L.; Balmer, W.; Krzemnicki, M.S. Spinel from Mogok, Myanmar—A Detailed Inclusion Study by Raman Microspectroscopy and Scanning Electron Microscopy. *J. Gemmol.* **2019**, *36*, 418–435. [CrossRef]
53. Huong, L.T.-T.; Häger, T.; Hofmeister, W.; Hauzenberger, C.; Schwarz, D.; Van Long, P.; Wehrmeister, U.; Khoi, N.N.; Nhung, N.T. Gemstones from Vietnam: An Update. *Gems Gemol.* **2012**, *48*, 158–176. [CrossRef]
54. Kruzslicz, A.B.; Nasdala, L.; Wildner, M.; Škoda, R.; Redhammer, G.J.; Hauzenberger, C.; Wanthanachaisaeng, B. Black Spinel—A Gem Material from Bo Phloi, Thailand. *J. Gemmol.* **2020**, *37*, 66–79. [CrossRef]
55. Htoo, K.M.; Khin, T.; Htoon, S. Study on Physical Properties and Chemical Composition of Some Myanmar Gems. *J. Myanmar Acad. Arts Sci.* **2004**, *2*, 173–178.
56. Azer, C.; Ramadan, A.R.; Ghaly, G.; Ragai, J. Preparation and Characterization of Cobalt Aluminate Spinels $CoAl_2O_4$ Doped with Magnesium Oxide. *Adsorpt. Sci. Technol.* **2012**, *30*, 399–407. [CrossRef]
57. Zhang, D.; Wang, C.; Liu, Y.; Shi, Q.; Wang, W.; Zha, Y. Green and red photoluminescence from $ZnAl_2O_4$:Mn phosphors prepared by sol—gel method. *J. Lumin.* **2012**, *132*, 1529–1531. [CrossRef]
58. Bakhmetyev, V.V.; Lebedev, L.A.; Malygin, V.V.; Podsypanina, N.S.; Sychov, M.M.; Belyaev, V.V. Effect of Composition and Synthesis Route on Structure and Luminescence of $NaBaPO_4:Eu^{2+}$ and $ZnAl_2O_4:Eu^{3+}$. *JJAP Conf. Proc.* **2016**, *4*, 011104. [CrossRef]
59. Tshabalala, K.G.; Nagpure, I.M.; Swart, H.C.; Ntwaeaborwa, O.M.; Cho, S.H.; Park, J.-K. Enhanced green emission from UV down-converting Ce^{3+}–Tb^{3+} co-activated $ZnAl_2O_4$ phosphor. *J. Vac. Sci. Technol. B* **2012**, *30*, 031401. [CrossRef]
60. Kumar, M.; Natarajan, V.; Godbole, S.V. Synthesis, characterization, photoluminescence and thermally stimulated luminescence investigations of orange red-emitting Sm^{3+}-doped $ZnAl_2O_4$ phosphor. *Bull. Mater. Sci.* **2014**, *37*, 1205–1214. [CrossRef]
61. Kumaria, P.; Dwivedi, Y.; Bahadur, A. Analysis of bright red-orange emitting Mn^{2+}:$ZnAl_2O_4$ spinel nanophosphor. *Optik* **2018**, *154*, 126–132. [CrossRef]
62. Strek, W.; Deren, P.; Bednarkiewicz, A.; Zawadzki, M.; Wrzyszcz, J. Emission properties of nanostructured Eu^{3+} doped zinc aluminate spinels. *J. Alloys Compd.* **2000**, *300–301*, 456–458. [CrossRef]
63. Belyaev, A.; Basyrova, L.; Sysoev, V.; Lelet, M.; Balabanov, S.; Kalganov, V.; Mikhailovski, V.; Baranov, M.; Stepanidenko, E.; Vitkin, V.; et al. Microstructure, doping and optical properties of Co^{2+}:$ZnAl_2O_4$ transparent ceramics for saturable absorbers: Effect of the ZnF_2 sintering additive. *J. Alloys Compd.* **2020**, *829*, 154514. [CrossRef]
64. Kumar, M.; Mohapatra, M. A case study of energy transfermechanism from uraniumto europium in $ZnAl_2O_4$ spinel host by photoluminescence spectroscopy. *Spectrochim. Acta Part A Mol. Biomol. Spectrosc.* **2016**, *159*, 42–47. [CrossRef]
65. Sumathi, S.; Kavipriya, A. Structural, optical and photocatalytic activity of cerium doped zinc aluminate. *Solid State Sci.* **2017**, *65*, 52e60. [CrossRef]

66. Luchechko, A.; Zhydachevskyy, Y.; Ubizskii, S.; Kravets, O.; Popov, A.I.; Rogulis, U.; Elsts, E.; Bulur, E.; Suchocki, A. Afterglow, TL and OSL Properties of Mn^{2+}-doped $ZnGa_2O_4$ Phosphor. *Sci. Rep.* **2019**, *9*, 9544. [CrossRef]
67. Mykhailovych, V.; Kanak, A.; Cojocaru, Ş.; Chitoiu-Arsene, E.-D.; Palamaru, M.N.; Iordan, A.-R.; Korovyanko, O.; Diaconu, A.; Ciobanu, V.G.; Caruntu, G.; et al. Structural, Optical, and Catalytic Properties of $MgCr_2O_4$ Spinel-Type Nanostructures Synthesized by Sol–Gel Auto-Combustion Method. *Catalysts* **2021**, *11*, 1476. [CrossRef]
68. Zhai, B.-G.; Huang, Y.-M. Green Afterglow of Undoped $SrAl_2O_4$. *Nanomaterials* **2021**, *11*, 2331. [CrossRef]
69. Web Site of Ertec Poland. Available online: www.ertec.pl (accessed on 20 July 2019).